American Welding Society®

SUPPLEMENT TO THE *WELDING JOURNAL*, APRIL 2024
Sponsored by the American Welding Society

WELDING RESEARCH

Effect of Wire Preheat and Feed Rate in X80 Steel Laser Root Welds: Part 1 — Microstructure

The effects of using hot-wire-fed laser welding to promote the formation of acicular ferrite in X80 welds were investigated

BY H. YANG, J. CHEN, N. HUDA, X. ZHAO, AND A.P. GERLICH

Abstract

Laser welding with cold versus hot wire feed was employed as a root pass to weld X80 pipeline steel. The influences of wire feed rate and preheat on the fusion zone microstructure were investigated. Increasing the wire feed rate helped generate acicular ferrite in the weld metal, and preheating the wire further suppressed the formation of bainite. The acicular ferrite in the upper region of the fusion zone was finer than that in the lower region, which was due to an increase in nucleation sites available. Five fill and cap passes were applied by gas metal arc welding to fill the remaining top part of the groove. Compared to arc welding with a higher heat input, laser welding led to finer prior austenite grains and smaller bainite packet size in the coarse-grained heat-affected zone and limited the formation of martensite-austenite constituents in the inter-critically reheated coarse-grained heat-affected zone.

Keywords

- Hot-Wire Laser Welding
- X80 Pipeline Steel
- Acicular Ferrite
- Bainite
- Heat-Affected Zone
- Martensite-Austenite Constituents

https://doi.org/10.29391/2024.103.009

Introduction

The rapid expansion of industrial activities has brought about a continuous increase in energy demand. Though renewable energy sources such as wind, hydro, tidal, and nuclear energy have expanded in recent years, fossil fuels, including petroleum, natural gas, and coal, still account for over 80% of global energy consumption in 2021 (Ref. 1). Long-distance transportation of oil and gas between the source and storage areas requires high-integrity pipelines with excellent strength and toughness. In the modern energy industry, pipes are made of high-strength low alloy (HSLA) steels due to their superior performance (Ref. 2). The traditional arc welding methods, such as shield metal arc welding (SMAW), submerged arc welding (SAW), and gas metal arc welding (GMAW), usually require long processing time and skilled labor, which limits productivity and weld quality.

Over recent years, the cost and size of high-power laser systems have dropped, which has attracted research interest in laser welding of pipeline steels. Laser beam welding (LBW) using a high energy density source is a promising method for joining thick plates due to its deep penetration and travel speed, enabling low heat input with minimal heat affected zone (HAZ) (Ref. 2). One of the main drawbacks of autogenous laser welding is the poor gap bridging ability, often requiring a gap of less than 10% of the plate thickness (Refs. 3–5). Alternatively, as demonstrated by Steen et al. (Ref. 6) in the 1980s, hybrid laser-arc welding (HLAW) is a more gap-tolerant technique for the welding of thick plates, combining the advantages of both laser and arc heat sources, which provides both deep penetration and good gap-bridging ability. One technical difficulty of HLAW is that an inhomogeneous weld metal microstructure can form along the through-thickness direction since the poor penetrating ability of the arc limits

Table 1 — Chemical Composition of X80 Steel (wt-%)

Chemical Composition of X80 Steel Used in This Work									
Element	C	Mn	Si	Ni	Cu	Mo	Ti	Nb	Fe
Wt-%	0.051	1.73	0.18	0.13	0.12	0.21	0.01	0.04	Bal.
Chemistry Range of X80 Steel Prescribed by API 5L									
Element	C	Mn	Si	Ni	Cu	Mo	Nb + Ti + V		Fe
Wt-%	0.12 max	1.85 max	0.45 max	1.00 max	0.5 max	0.5 max	0.15 max		Bal.

the mixing of the filler materials throughout the melt pool. During HLAW of carbon steels, the upper 'arc fusion zone' contains most of the wire feed material that helps promote the formation of a tough microstructure such as acicular ferrite, but the root 'laser fusion zone' is deficient in the filler metal elements and may contain hard and brittle phases like bainite due to the high cooling rate being applied to the base metal chemistry (Ref. 7).

Another method to improve the performance of laser welding is to feed wire during the welding process, usually with the laser in a conduction mode (Ref. 8). Feeding additional wire helps improve the gap-bridging ability and can also modify the chemistry and microstructure of the weld metal, which would further influence the mechanical properties of the weld. Due to the excellent penetration of the laser, the groove can be very narrow, thus reducing the total weld passes and required filler material, which is beneficial to improve productivity in comparison with arc welding (Ref. 9). Guo et al. (Ref. 10) compared multi-pass ultra narrow gap laser welding (NGLW) with the GMAW process during the welding of 8-mm-thick S960 high-strength steel and found the total heat input and required filler material using GMAW was 6 times that of NGLW; meanwhile, the travel speed of NGLW was 1.5 times that of GMAW.

An external power supply can also be added to preheat the wire, which facilitates hot-wire laser welding (HWLW) (Ref. 11). By running an electric current through the wire, the filler material can be preheated to a temperature near the melting point, which helps increase the deposition rate and productivity during laser welding (Ref. 12). Wei et al. (Ref. 12) proposed that the preheat of the filler wire increased the welding stability and improved the weld seam formation, while reducing the total heat input needed from the laser, with a maximum energy saving of 16% over the cold wire laser welding process. Ohnishi et al. (Ref. 13) obtained sound, fully penetrated welds over a range of gaps from 0 to 0.4 mm when performing hot wire laser welding with a 16kW laser power on 12 mm thick carbon steels. Sun et al. (Ref. 14) reported that the distribution of wire elements was uniform from the top to the bottom of a 3 mm thick hot-wire laser-welded butt joint. Metzbower et al. (Ref. 15) reported that during laser welding of HY80 steel, instead of obtaining an untempered martensitic microstructure in the autogenous welds, the introduction of a hot-wire feed metal could modify the weld

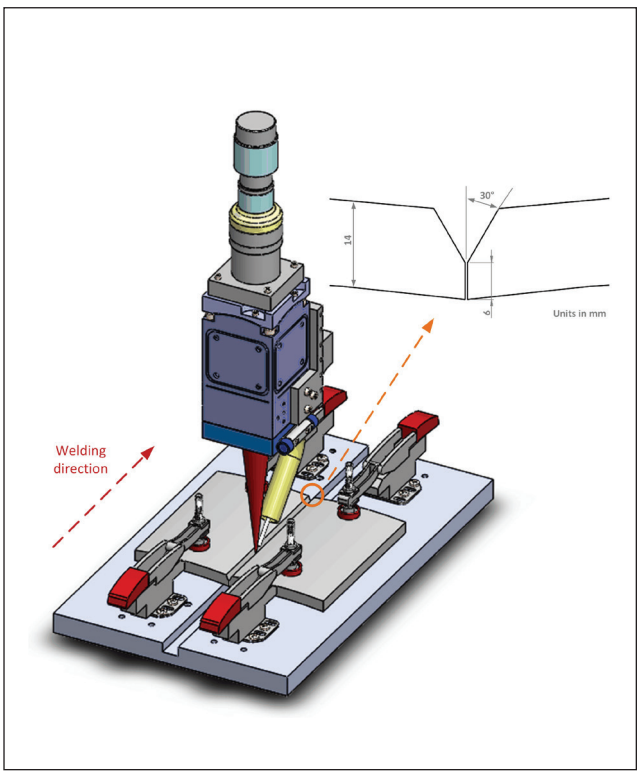

Fig. 1 — Laser welding experimental set-up with wire feed.

metal microstructure depending on the feed rate. A slow wire feed resulted in a mixed martensite-bainite structure, whereas a fast feed resulted in a microstructure with primarily acicular ferrite. They also suggested that the addition of hot wire had an effect equivalent to using a preheated substrate during welding, which would reduce the cooling rate in the fusion zone (FZ).

In this first part of the study presented, the effects of wire feed rate (WFR) and the preheat of the wire on the fusion zone microstructure during laser keyhole welding of X80 pipeline steel were investigated. In the present work, a high penetration laser weld root pass is combined with GMAW fill passes to achieve a compromise between the benefit of a

Table 2 — Chemical Composition of ER70S-6 Wire (wt-%)

Element	C	Mn	Si	Ni	Cu	Mo	Ti + Zr	Al	Fe
Wt-%	0.06-0.12	1.45-1.65	0.90-1.00	0.15 max	0.30 max	max	0.15 max	0.02 max	Bal.

Table 3 — Welding Parameters Used in This Work

Sample Number	Laser Power P (kW)	Welding Speed v (m/min)	Wire Feed Rate WFR (m/min)	Hot Wire Preheat Power P_{wire} (kW)	Root Opening d (mm)	Defocused Distance D_f (mm)	Total Linear Heat Input *HI* (J/mm)
1	8	1	—	—	0	-3	480
2	8	1	4	—	0	-3	480
3	8	1	6	—	0.4	-3	480
4	8	1	6	0.3	0.4	-3	498
5	8	1	12	—	0.4	-3	480
6	8	1	12	0.5	0.4	-3	510

higher productivity laser process, while potentially improving the properties of the laser weld zone by tempering from later passes. The heat input and travel speed between root laser welding and the GMAW process were compared to evaluate the advantage of laser welding in productivity. The HAZ obtained during different welding processes was also compared. In a second paper, the mechanical properties of the joint regions were studied in more detail.

Experimental Procedures

Welding Equipment and Materials

The experimental set-up for the wire-fed laser welding process is shown in Fig. 1. An IPG YLS-8000 fiber laser with a maximum power output of 8 kW was used in this work, with a focal length of 300 mm, a wavelength of 1070 nm, a beam parameter product of 3.5 mm*mrad, and a focused spot size of 1.2 mm. A Lincoln Electric Power Wave L500 power supply was used to preheat and feed the wire in front of the laser. The laser welding head was equipped with a hot-wire torch and positioned by a Fanuc R-301iB Plus six-axis industrial robot system.

The base metal was taken from an X80 pipeline with dimensions of 250 mm × 120 mm × 14 mm and an internal radius of 470 mm, with a chemical composition given in Table 1. ER70S-6 carbon steel welding wire was used with a diameter of 0.9 mm, with the typical wire chemistry provided in Table 2. As shown in Fig. 1, the edge of the plate was machined with a 30-deg bevel and a 6 mm root height. Before welding, the oxides on the plate surfaces were removed by sandblasting, and the plates were tack-welded together to ensure accurate positioning and minimize distortion during welding.

Welding Test Design

Cold and hot wire laser welding was performed for the root pass, with the welding parameters listed in Table 3. The laser was the only heat source during autogenous laser welding and cold-wire laser welding process. Meanwhile, an external power supply was used to preheat the wire by running an electrical current through it during hot-wire laser welding, such that 0.3 to 0.5 kW were applied to the wire during deposition, depending on the wire feed speed. For the calculated temperature rise based on the wire heat capacity, a 0.3 kW preheat power combined with a WFR of 6 m/min will lead to an estimated temperature increase of around 1200°C, while a 0.5 kW power combined with a WFR of 12 m/min will lead to a temperature increase of around 1400°C. With the high WFRs of 6 m/min and 12 m/min, a 0.4 mm root opening was used to help accommodate more filler material. The remaining part of the groove was filled with five passes of arc welds with the same ER70S-6 wire, each pass of which with a WFR of 6.9 m/min, a travel speed of 0.13 m/min, a welding current of around 143.7 A and a welding voltage of 19 V, which led

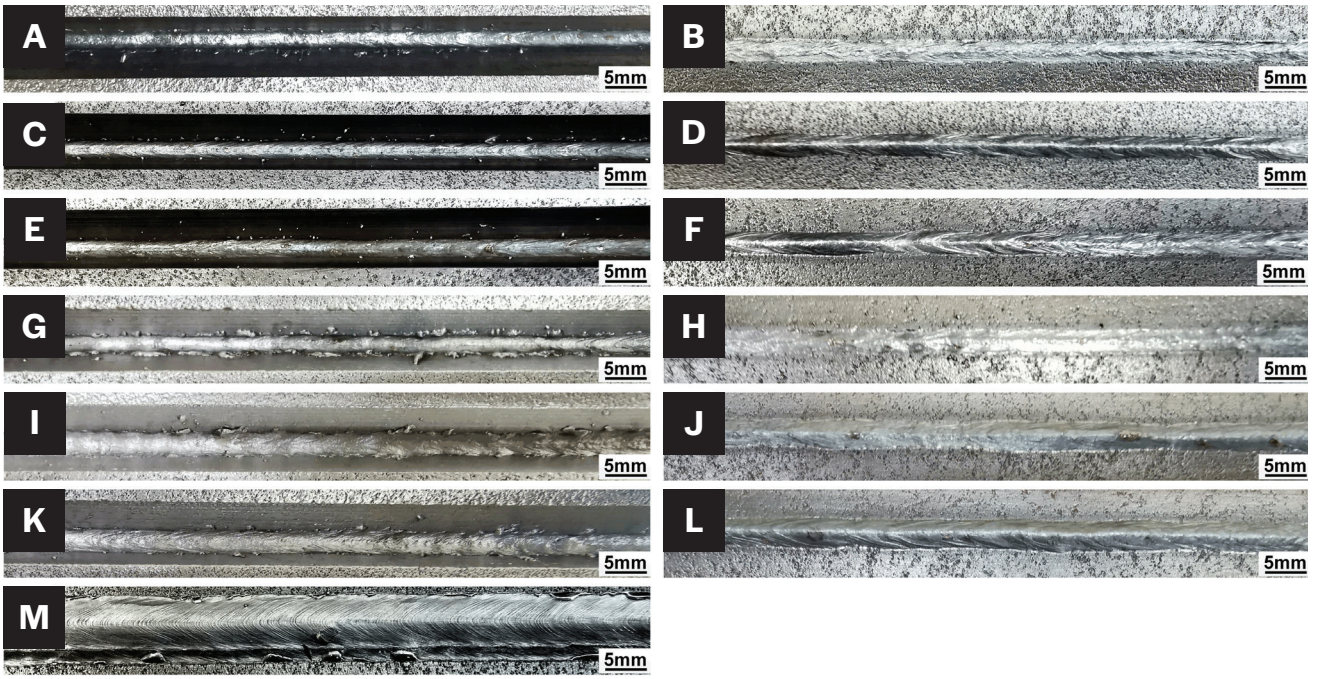

Fig. 2 — Weld surfaces morphologies: A and B — Top and bottom surfaces of autogenous laser weld; C and D — top and bottom surfaces of cold-wire laser weld with a WFR of 4 m/min; E and F — top and bottom surfaces of cold-wire laser weld with a WFR of 6 m/min; G and H — top and bottom surfaces of hot-wire laser weld with a WFR of 6 m/min; I and J — top and bottom surfaces of cold-wire laser weld with a WFR of 12 m/min; K and L — top and bottom surfaces of hot-wire laser weld with a WFR of 12 m/min; M — top surface of cap arc weld.

to a linear heat input of 1.30 KJ/mm, higher than that of the cold-wire feed laser welding process, which is 0.48 KJ/mm. The shielding gas used for the laser and arc welding process are pure Ar and mixed gas (85% Ar + 15% CO_2), respectively, with the same flow rate of 18 L/min.

Microstructure Analysis

After welding, the cross-sectional samples were cut out and polished for microstructural analysis and microhardness tests. The samples were etched with Nital, a mixture of 5% nitric acid and 95% ethanol, for 5 s to reveal the microstructure based on ASTM E407. To identify the weld dimensions, macrographs were taken under a stereoscope. An Olympus BX51 optical microscope (OM) and a Zeiss Ultra scanning electron microscope (SEM) were utilized to characterize the microstructure with various magnifications.

Results and Discussion

Weld Morphologies

All completed welded joints had the same number of passes, including the root laser weld and five passes of fill arc welds. The top and root surfaces of the laser welds and the cap arc weld are shown in Fig 2. Crack-free, narrow, and continuous root welds were produced with the laser, in comparison with a much wider cap weld resulting from the lower energy density and larger weld pool from the arc heat source. Cross-section morphologies of the laser welds shown in Fig. 3A–F demonstrate that the substrates were completely penetrated. The laser welds had high depth-to-width ratios which is a key feature of laser keyhole mode welding with a high beam power density, and the increase of weld height was found when the wire feed rate increased from 0 to 12 m/min. Interestingly, with a commonly used GMAW groove design (with a 30-deg included angle) which is suggested in the CSA-Z662 pipeline joining standard, five passes of arc welds were required to achieve a comparable weld height with the root laser weld, while each pass of GMAW had about 3 times higher heat input that of the root LBW process, as shown in Fig. 3G. The cumulative heat input of GMAW was around 15 times that of the laser welding; however, the travel speed during root laser welding was about 7.7 times that of the single GMAW pass. This demonstrates the significant productivity advantage of laser welding over traditional arc welding techniques.

Fusion Zone Microstructure

The microstructure of the X80 HSLA steel substrate is shown in Fig. 4, which is composed of fine-grained ferrite and granular bainite. The presence of granular bainite, where the martensite-austenite (MA) constituents, decomposed MA, or cementite precipitation dispersed in bainitic ferrite matrix (Ref. 16), as shown in the high-magnification SEM image of

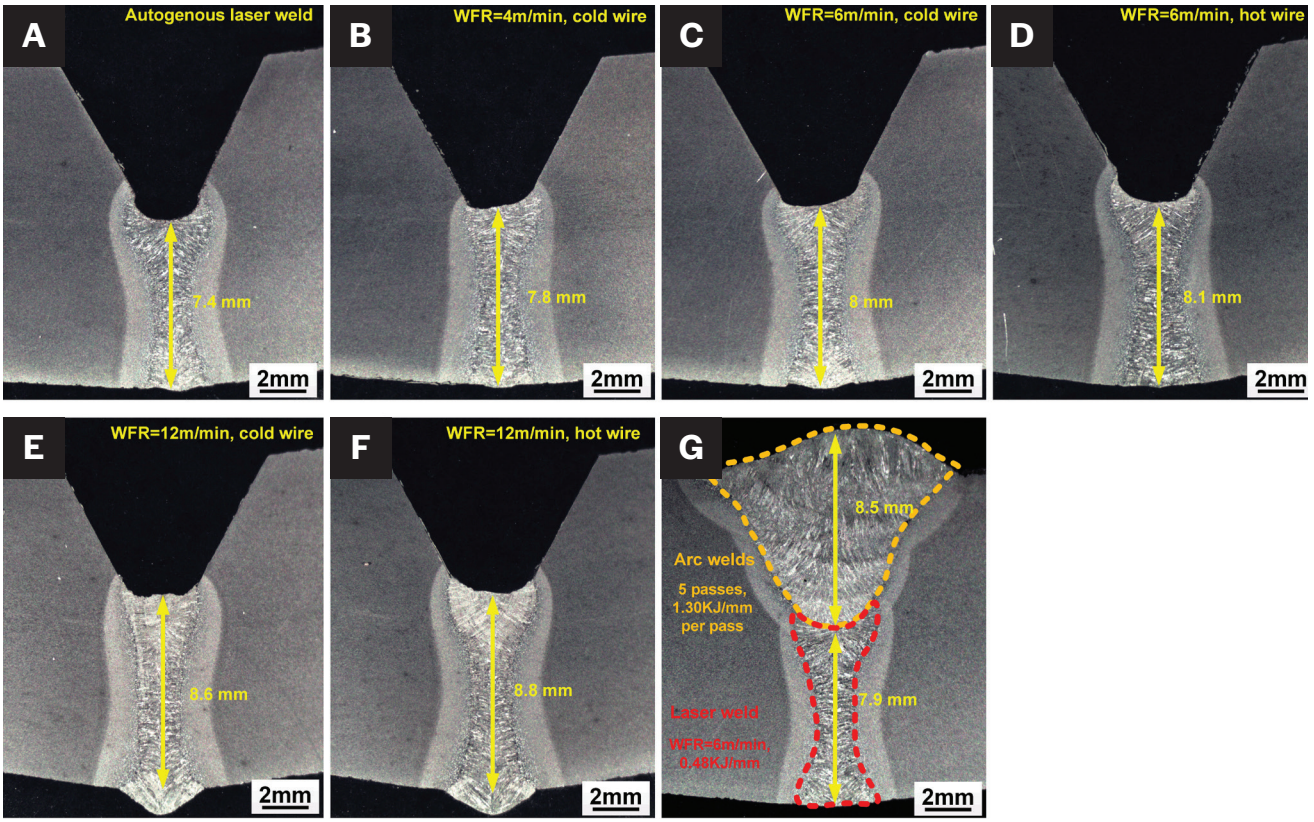

Fig. 3 — Cross-section morphologies: A — Autogenous laser weld; B — cold-wire laser weld, WFR = 4 m/min; C — cold-wire laser weld, WFR = 6 m/min; D — hot-wire laser weld, WFR = 6 m/min; E — cold-wire laser weld, WFR = 12 m/min; F — hot-wire laser weld, WFR = 12 m/min; G — final joint with root laser weld and 5 passes of filler GMAW weld.

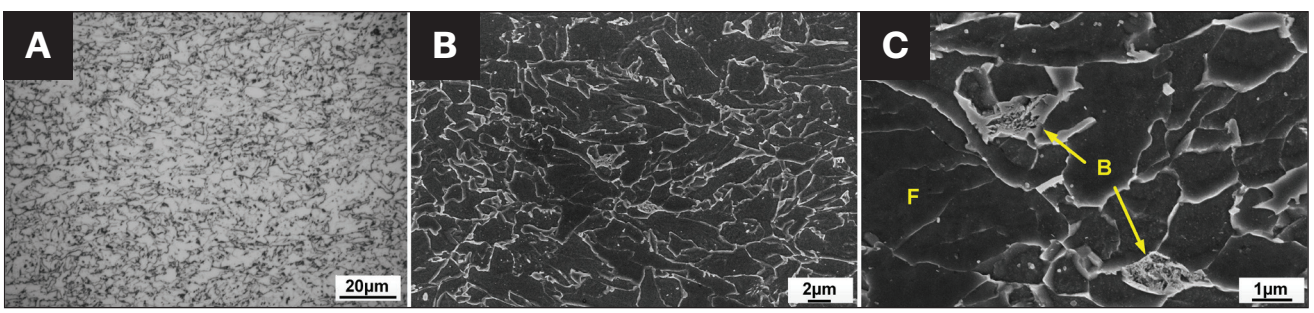

Fig. 4 — Microstructure of X80 base metal: A — Optical micrograph; B and C — SEM micrograph.

Fig. 4C. During laser welding, the wire was fed from the top side of the root face, which could lead to an uneven distribution of filler material and microstructure inhomogeneity along the thickness direction. OM images in Fig. 5 show the microstructure of the upper region of the laser fusion zone with different welding parameters. The FZ of the autogenous laser weld mainly contained bainite (B), resulting from a high cooling rate, as presented in Fig. 5A. In contrast, the feed of wire helped generate acicular ferrite (AF) in the upper region of the FZ. Feeding ER70S-6 filler material may introduce non-metallic inclusions originating from alloying additions and impurities into the weld metal, and some of these provide favorable nucleation sites for the formation of intragranular AF (Refs. 17–20). With a higher WFR, the increasing number of non-metallic inclusions provided more nucleation sites which resulted in the formation of a larger amount of fine-grained AF. On the other hand, preheating the wire reduced the cooling rate (Refs. 15, 21), which limited the formation of bainite. As a result, the upper region of FZ in the hot-wire laser weld with the highest WFR of 12 m/min contained mostly fine AF but little bainite, as shown in Fig. 5F.

The microstructure of the lower region of the laser FZ is shown in Fig. 6. The lower region of FZ in the autogenous laser weld was mainly made up of bainite, which was similar to the

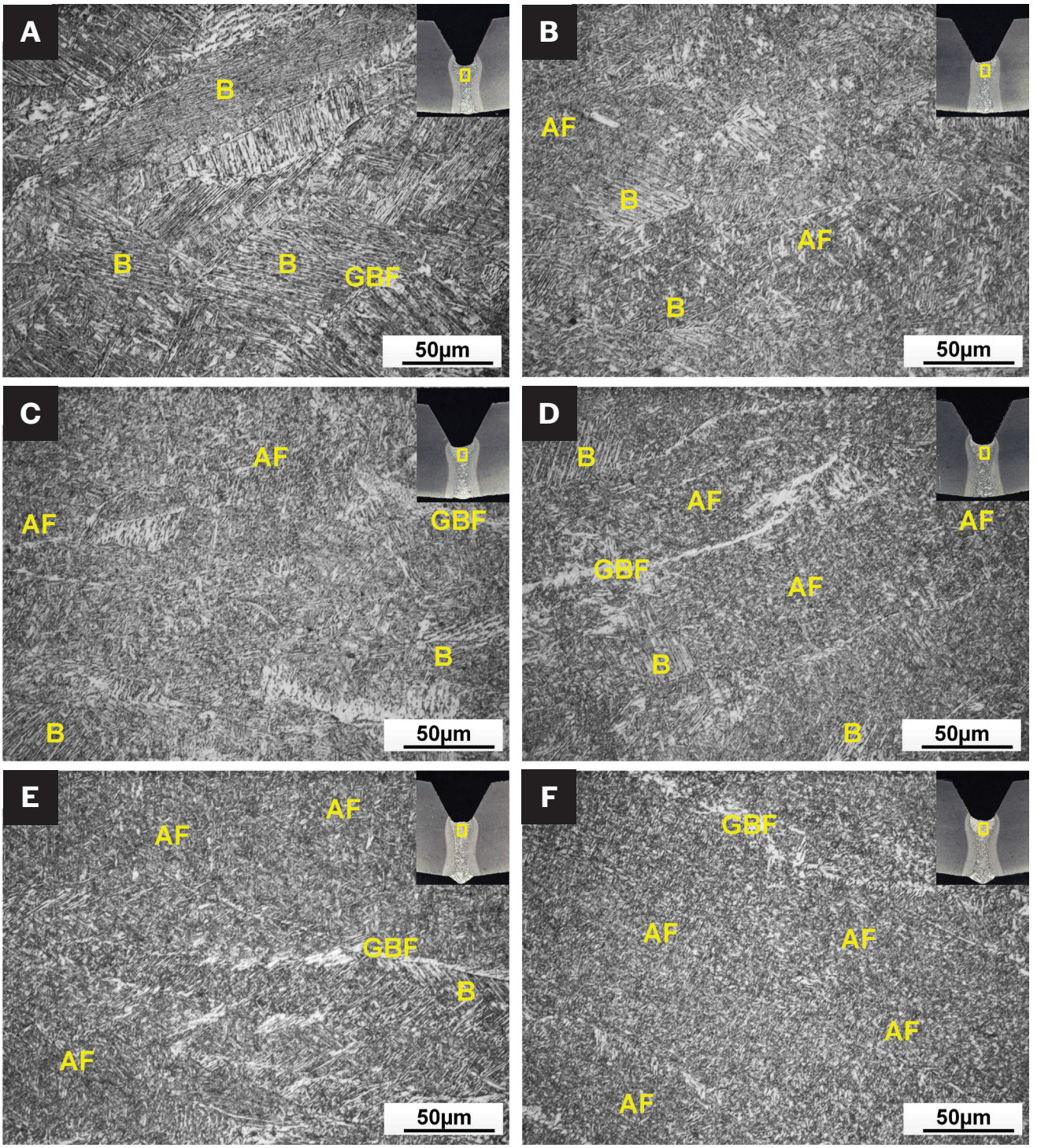

Fig. 5 — Optical micrographs showing the microstructure of upper region of the FZ: A — Autogenous laser weld; B — cold-wire laser weld, WFR = 4 m/min; C — cold-wire laser weld, WFR = 6 m/min; D — hot-wire laser weld, WFR = 6 m/min; E — cold-wire laser weld, WFR = 12 m/min; F — hot-wire laser weld, WFR = 12 m/min.

upper region due to a negligible change in the chemical composition, as shown in Fig. 6A. Compared to the autogenous laser weld, more AF formed in the lower region of the FZ with a wire feed due to the increased alloying with elements such as Ti, which is reported to promote the formation of AF (Refs. 17, 19), and the presence of a root opening which provided a channel for the delivery of filler metal to the root region.

The high magnification SEM images in Fig. 7 provide a clearer view of the FZ microstructure of the autogenous laser weld, and the hot-wire weld with a WFR of 12 m/min. Predominantly bainite was formed in the FZ of the autogenous laser

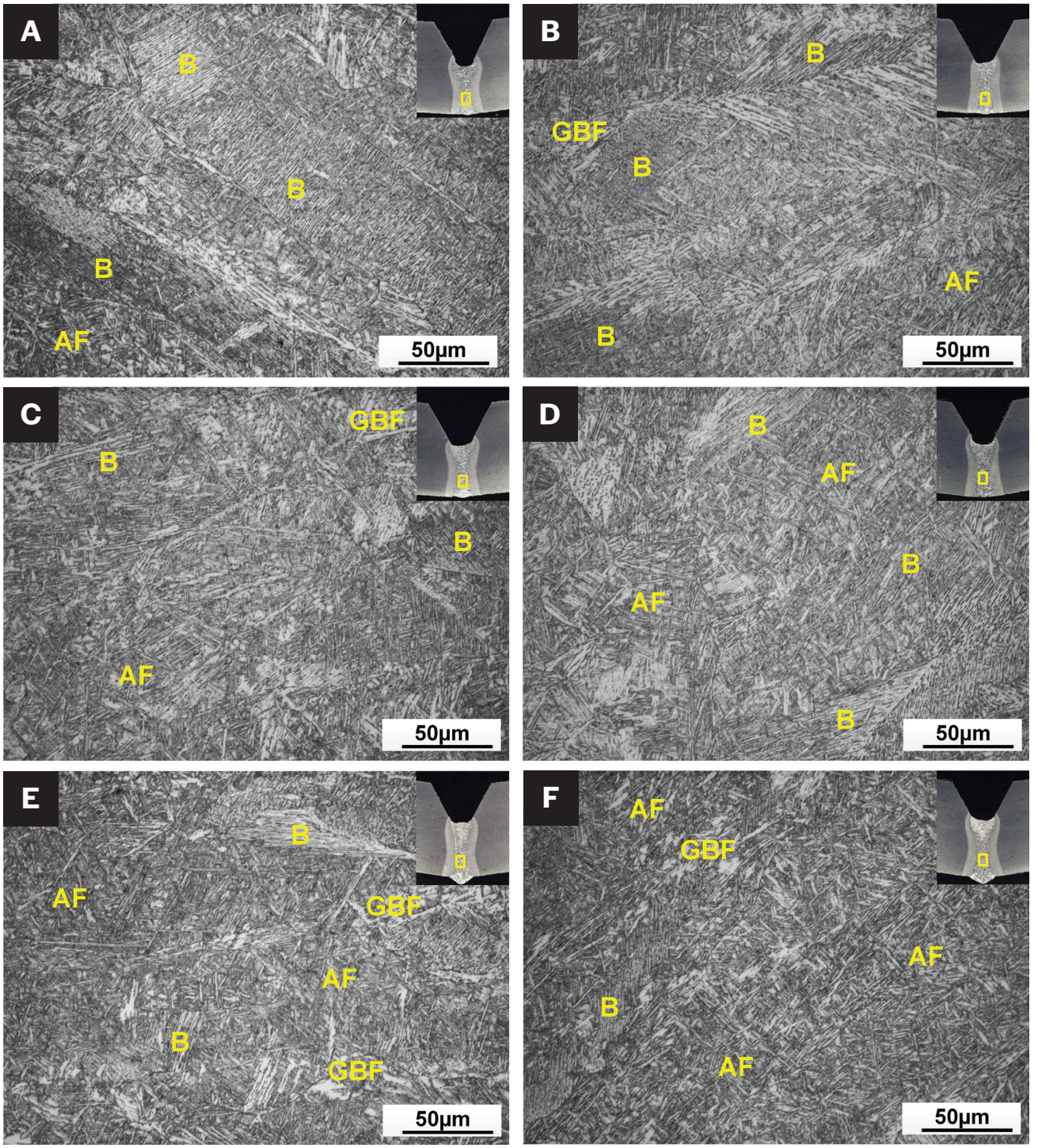

Fig. 6 — Optical micrographs showing the microstructure of lower region of the FZ: A — Autogenous laser weld; B — cold-wire laser weld, WFR = 4 m/min; C — cold-wire laser weld, WFR = 6 m/min; D — hot-wire laser weld, WFR = 6 m/min; E — cold-wire laser weld, WFR = 12 m/min; F — hot-wire laser weld, WFR = 12 m/min.

weld, as shown in Fig. 7A–D. Meanwhile, the wire additions promoted the formation of acicular ferrite, as shown clearly by the basket-weave morphology of grains in Fig. 7E–H. The acicular ferrite in the upper region of FZ was finer than that in the lower region, which might be due to an increase in nucleation sites available, which would be expected based on reduced mixing and transport of alloying elements to the bottom of the weld pool. Compared to the upper region of FZ, more bainite but less AF was found in the lower region of FZ in the hot-wire weld, which also resulted from the less filler material and alloying elements reaching the root region.

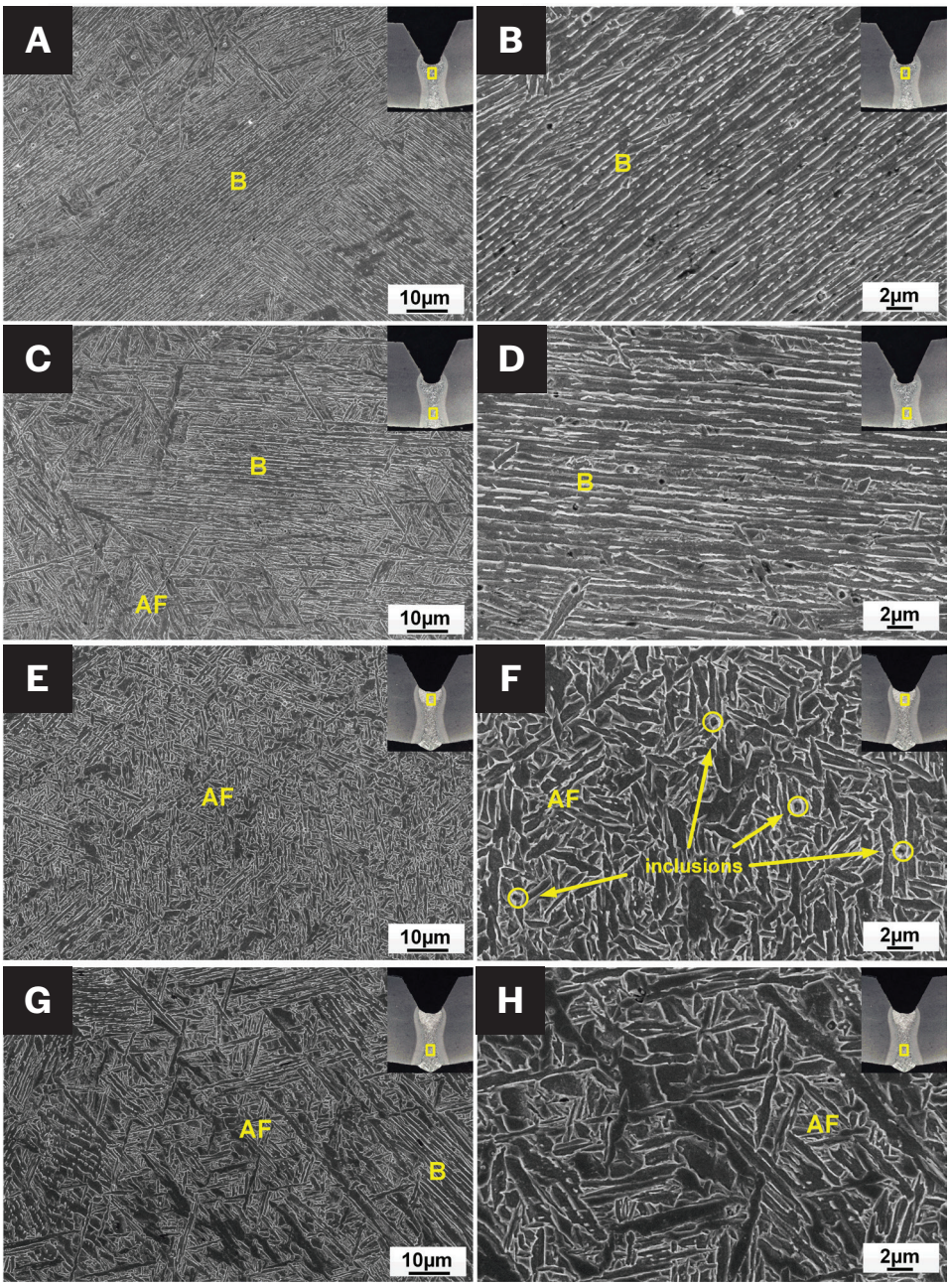

Fig. 7 — SEM micrographs indicating the presence of bainite (B) and acicular ferrite (AF) in: A and B — Upper region of the FZ in autogenous laser weld; C and D — lower region of the FZ in autogenous laser weld; E and F — upper region of the FZ in hot-wire laser weld with a WFR of 12 m/min; G and H — lower region of the FZ in hot-wire laser weld with a WFR of 12 m/min.

Heat-Affected Zone Microstructure

Figures 8 and 9 show the OM and SEM images of the heat-affected zone of the laser weld, respectively. The HAZ sub-regions exhibited different grain sizes and microstructures resulting from various peak temperatures and cooling rates. Sub-zones of the HAZ can be distinguished, which are delineated in Fig. 8A, and these were further examined at higher magnification. The coarse-grained heat-affected zone (CGHAZ) mainly consisted of bainite, as shown in Figs. 8B and 9A–B. The CGHAZ adjacent to the FZ experienced a high peak temperature that promoted the growth of prior austenite grain, which is beneficial to the formation of low-temperature transformation products like bainite or martensite (Refs. 22, 23). The peak temperature in the fine-grained heat affected zone (FGHAZ) was still higher than the full austenization temperature (A_{r3}), but lower than the dissolution temperature of most precipitates existing in the HSLA steels produced through thermo-mechanically controlled processing (TMCP) (Ref. 23). The pinning effect of the precipitates would retard

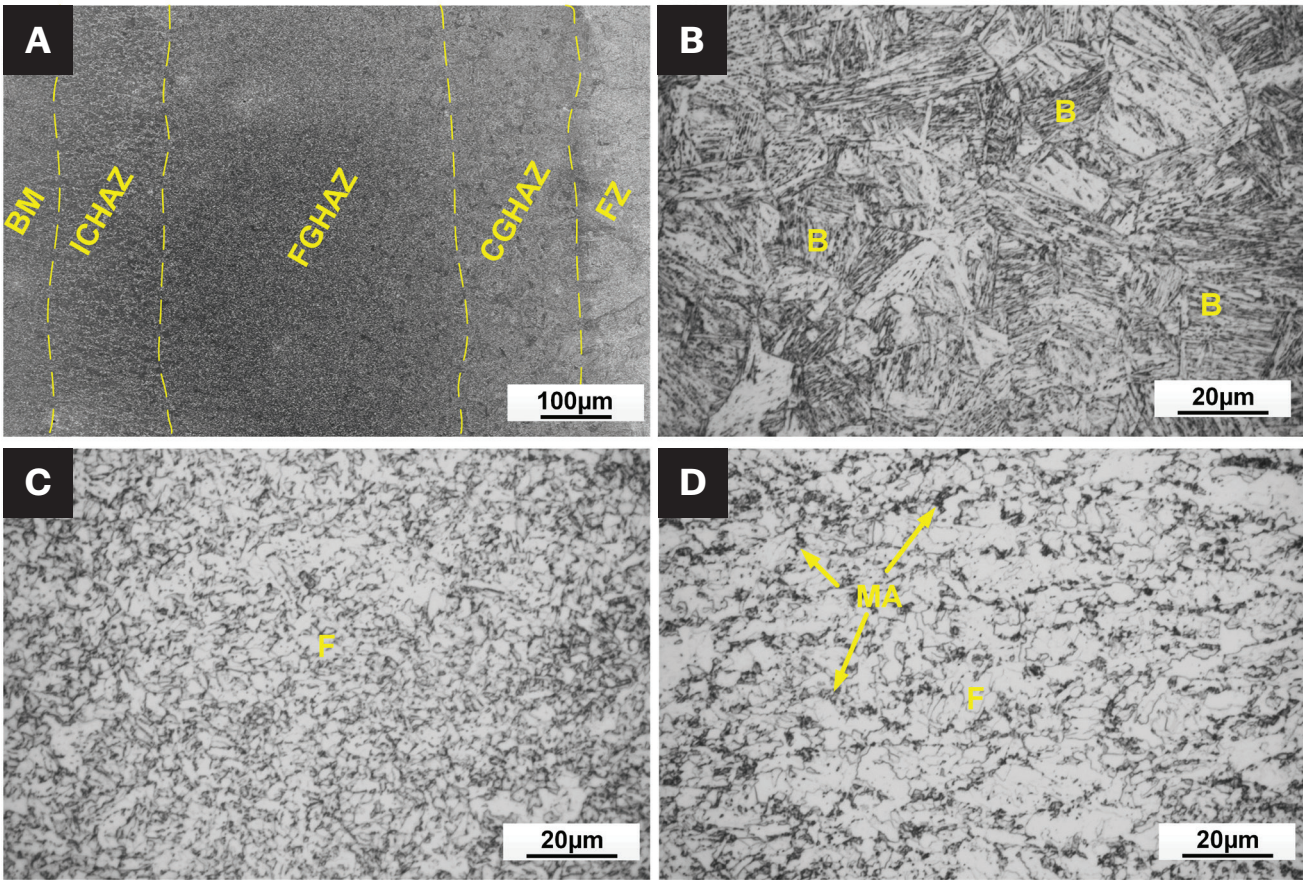

Fig. 8 — A — Sub-zones in the HAZ of laser weld; B — optical micrograph of CGHAZ, cold-wire laser weld, WFR = 6 m/min; C — optical micrograph of FGHAZ, cold-wire laser weld, WFR = 6 m/min; D — optical micrograph of ICHAZ, cold-wire laser weld, WFR = 6 m/min.

the growth of austenite grains, which provided more grain boundaries as favorable nucleation sites for ferrite (Ref. 22). As a result, the FGHAZ was made up of fine-grained ferrite, shown in Figs. 8C and 9C–D. Martensite-austenite (MA) constituents were found in the inter-critical heat affected zone (ICHAZ) with a peak temperature between A_{r1} and A_{r3} where partial austenization occurred, as presented in Fig. 8D and 9E–F. Upon cooling from this temperature range, some carbon-enriched austenite was retained at room temperature or partially transformed to martensite below the martensite start temperature (M_s), which led to the formation of blocky MA (Ref. 24).

The formation of MA was also found in the inter-critically reheated (ICR) CGHAZ when a second weld pass was applied over an existing weld pass. The second thermal cycle leads to the formation of multiple reheated HAZ, of which the ICRCGHAZ is often considered the weakest or most brittle region in a muti-pass weldment of pipeline steel due to the bainitic microstructure, large bainite packet size, along with the presence of second phase such as MA (Ref. 25). Fig. 10 shows the microstructure of CGHAZ formed by a single welding thermal cycle, and ICRCGHAZ formed by double thermal cycles of the arc and laser weld. The lower heat input during laser welding led to finer prior austenite grains and smaller bainite packet size in the CGHAZ, compared to that in the CGHAZ of the arc weld, as shown in Fig. 10A and 10E. The ICRCGHAZ of the arc weld formed when a second arc weld pass was applied over the existing arc weld pass; meanwhile, the ICRCGHAZ of the laser weld formed when the first pass of arc weld was applied over the root laser weld. Blocky MA constituents were found at the prior austenite grain boundaries in the ICRCGHAZ of both the arc and laser weld, as shown in Fig. 10B–D and 10F–H, respectively. Compared to GMAW, the deep penetration during laser welding reduced the total weld passes required and hence limited the formation of MA within the ICRCGHAZ. A smaller bainite packet size along with less MA in the ICRCGHAZ would be beneficial to the toughness of the HAZ in the laser weld.

Conclusions

The findings presented reveal the advantage of laser welding in productivity and the influence of filler material volume and preheat on the FZ microstructure during laser welding of X80 pipeline steel. The HAZ microstructure evolution in laser and arc welds was also discussed. In particular:

1. Compared to GMAW, laser welding had a significant advantage in productivity. To achieve a similar 8 mm weld

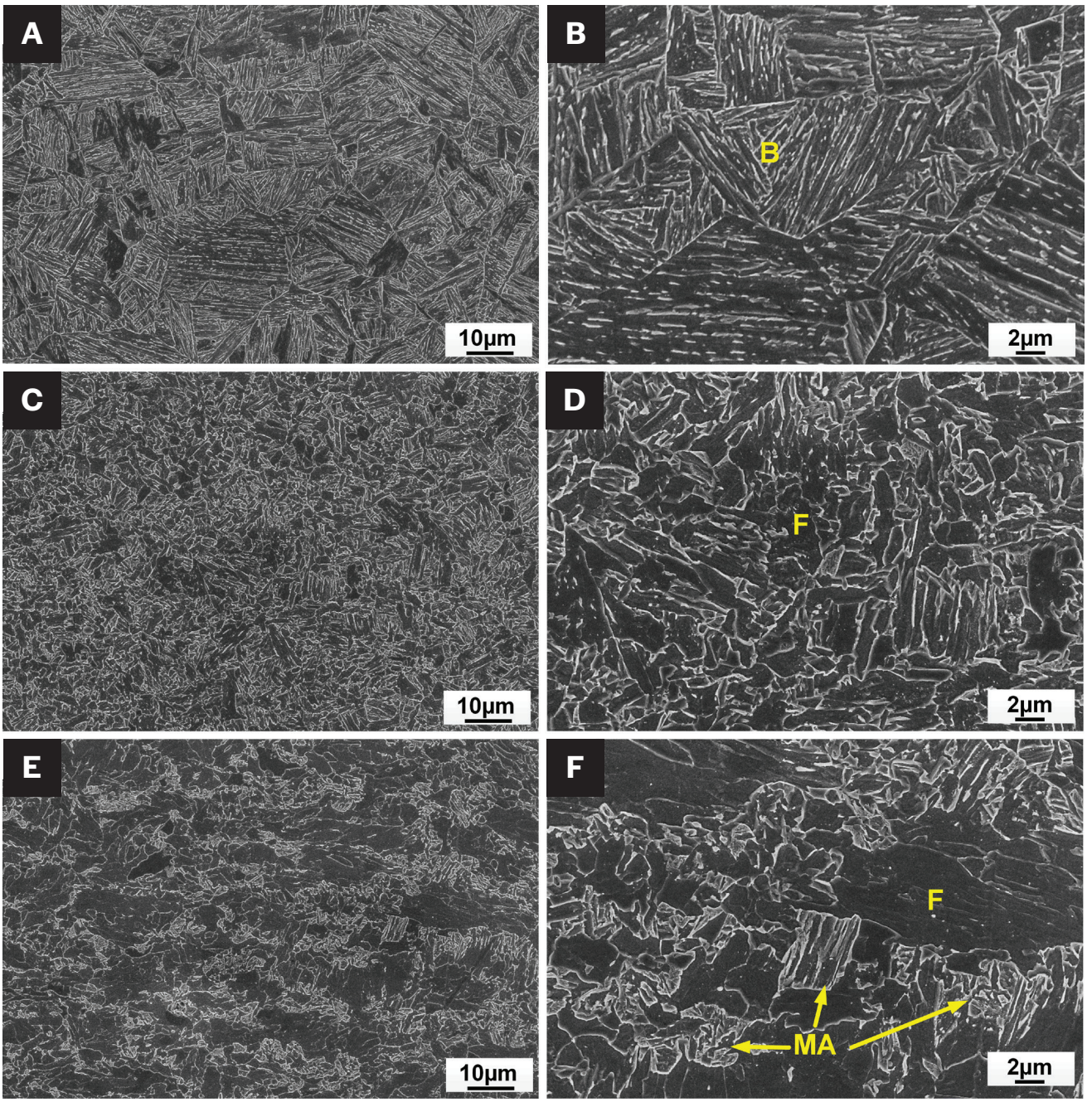

Fig. 9 — SEM micrographs of HAZ of cold-wire laser weld with a WFR of 12 m/min: A and B — CGHAZ; C and D — FGHAZ; E and F — ICHAZ.

height, the cumulative heat input of GMAW was around 15 times that of the laser welding; however, the travel speed of root laser welding was about 7.7 times that of the single GMAW pass.

2. Introducing ER70S-6 wire at a feed rate of 6 m/min helped generate acicular ferrite in the fusion zone by modifying the chemical composition. The formation of bainite in the weld metal can be limited by increasing the WFR to 12 m/min, along with resistively preheating the wire with a power of 0.5 kW. Compared to the autogenous laser weld with a bainitic microstructure, the upper region of the FZ in the hot-wire weld with a WFR of 12 m/min was mainly composed of acicular ferrite. The acicular ferrite in the upper region of FZ was finer than that in the lower region, which might be due to an increase in nucleation sites available.

3. The lower heat input during laser welding led to finer prior austenite grains and smaller bainite packet size in the CGHAZ, compared to that formed during GMAW. In comparison with GMAW, the deep penetration during laser welding reduced the total weld passes required, and hence limited the formation of MA within the ICRCGHAZ.

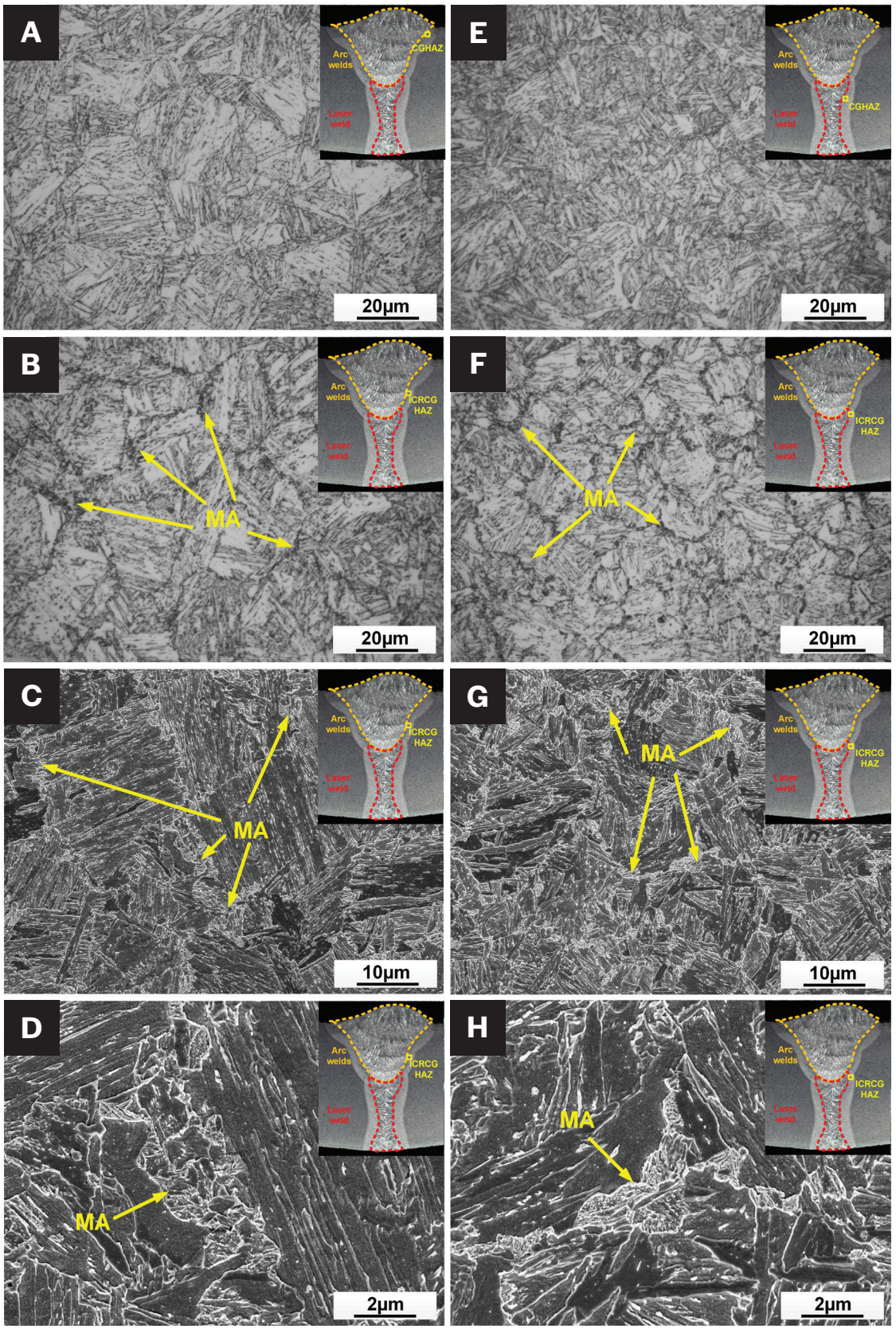

Fig. 10 — A — Optical micrograph of CGHAZ of arc weld; B — optical micrograph of ICRCGHAZ of arc weld; C and D — SEM micrographs of ICRCGHAZ of arc weld; E — optical micrograph of CGHAZ of cold-wire laser weld with a WFR of 6 m/min; F — optical micrograph of ICRCGHAZ of cold-wire laser weld with a WFR of 6 m/min; G and H — SEM micrograph of ICRCGHAZ of cold-wire laser weld with a WFR of 6 m/min.

Acknowledgments

The authors wish to acknowledge the Natural Sciences and Engineering Research Council of Canada (NSERC), Natural Resources Canada, the Canada Foundation for Innovation (CFI), and TC Energy Corp. for their funding and support.

References

1. BP p.l.c. 2022. *BP Statistical Review of World Energy* 71st edition.

2. Yang, H., Chen, J., Huda, N., and Gerlich, A. P. 2022. Effect of beam wobbling on microstructure and hardness during laser welding of X70 pipeline steel. *Science and Technology of Welding and Joining* 27(5): 326–338. DOI: 10.1080/13621718.2022.2053395

3. Salminen, A. 2010. The filler wire – Laser beam interaction during laser welding with low alloyed steel filler wire. *Mechanika* 84(4): 67–74. DOI: 10.5755/j01.mech.84.4.15914

4. Lehner, C., Reinhart, G., and Schaller, L. 1999. Welding of die-casted magnesium alloys for production. *Journal of Laser Applications* 11(5): 206–210. DOI: 10.2351/1.521865

5. Lampa, C. 1995. Practical and theoretical aspects of laser welding. Ph.D. dissertation. Norrbotten County, Luleå University of Technology.

6. Steen, W. M. 1980. Arc augmented laser processing of materials. *Journal of Applied Physics* 51(11): 5636–5641.DOI: 10.1063/1.327560

7. Zhenglong, L., Caiwang, T., Yanbin, C., and Zhongshao, S. 2013. Microstructure and mechanical properties of fiber laser-metal active gas hybrid weld of X80 pipeline steel. *Journal of Pressure Vessel Technology* 135(1). DOI:10.1115/1.4006347

8. Näsström, J., Frostevarg, J., and Kaplan, A. F. H. 2017. Multipass laser hot-wire welding: Morphology and process robustness. *Journal of Laser Applications* 29(2): 022014. DOI: 10.2351/1.4983758

9. Ramakrishna R, V. S. M., Amrutha, P. H. S. L. R., Rahman Rashid, R. A., and Palanisamy, S. 2020. Narrow gap laser welding (NGLW) of structural steels—a technological review and future research recommendations. *The International Journal of Advanced Manufacturing Technology* 111(7-8): 2277–2300. DOI: 10.1007/s00170-020-06230-9

10. Guo, W., Li, L., Dong, S., Crowther, D., and Thompson, A. 2017. Comparison of microstructure and mechanical properties of ultra-narrow gap laser and gas-metal-arc welded S960 high strength steel. *Optics and Lasers in Engineering* 91: 1–15. DOI: 10.1016/j.optlaseng.2016.11.011

11. Näsström, J., Frostevarg, J., and Silver, T. 2015. Hot-wire laser welding of deep and wide gaps. *Physics Procedia* 78: 247–254. DOI: 10.1016/j.phpro.2015.11.035

12. Wei, H., Zhang, Y., Tan, L., and Zhong, Z. 2015. Energy efficiency evaluation of hot-wire laser welding based on process characteristic and power consumption. *Journal of Cleaner Production* 87: 255–262. DOI: 10.1016/j.jclepro.2014.10.009

13. Ohnishi, T., Kawahito, Y., Mizutani, M., and Katayama, S. 2013. Butt welding of thick, high strength steel plate with a high power laser and hot wire to improve tolerance to gap variance and control weld metal oxygen content. Science and Technology of Welding and Joining 18:314–322. DOI: 10.1179/1362171813Y.0000000108

14. Sun, Z., and Kuo, M. 1999. Bridging the joint gap with wire feed laser welding. *Journal of Materials Processing Technology* 87(1–3): 213–222. DOI: 10.1016/S0924-0136(98)00346-X

15. Metzbower, E. A., Bhadeshia, H. K. D. H., and Phillips, R. H. 1994. Microstructures in hot wire laser beam welding of HY 80 steel. *Materials Science and Technology* 10(1): 56–59. DOI: 10.1179/mst.1994.10.1.56

16. Zhou, Y., Jia, T., Zhang, X., Liu, Z., and Misra, R. D. K. 2015. Investigation on tempering of granular bainite in an offshore platform steel. *Materials Science and Engineering: A* 626: 352–361. DOI: 10.1016/j.msea.2014.12.074

17. Midawi, A. R. H., Santos, E. B. F., Huda, N., Sinha, A. K., Lazor, R., and Gerlich, A. P. 2015. Microstructures and mechanical properties in two X80 weld metals produced using similar heat input. *Journal of Materials Processing Technology* 226: 272–279. DOI: 10.1016/j.jmatprotec.2015.07.019

18. Prokić-Cvetković, R. M., Milosavljević, A. J., Sedmak, A. S., Popović, O. D., and Petronić, S. J. 2006. Formation of acicular ferrite on non-metallic inclusion in low-alloy welded joints. *Proceedings of 10th International Research/Expert Conference 'Trends in the Development of Machinery and Associated Technology* 1315–1318. Barcelona, Spain.

19. Beidokhti, B., Koukabi, A. H., and Dolati, A. 2009. Influences of titanium and manganese on high strength low alloy SAW weld metal properties. *Materials Characterization* 60(3): 225–233. DOI: 10.1016/j.matchar.2008.09.005

20. Babu, S. S. 2004. The mechanism of acicular ferrite in weld deposits. *Current opinion in solid state and materials science* 8(3–4): 267–278. DOI: 10.1016/j.cossms.2004.10.001

21. Li, S., Xu, W., Xiao, G., Zhou, Z., Su, F., and Feng, J. 2020. Effects of Sc on laser hot-wire welding performance of 7075 aluminum alloy. *Materials Research Express* 7(10): 106506. DOI: 10.1088/2053-1591/abbd0a

22. Lan, L., Chang, Z., and Fan, P. 2018. Exploring the difference in bainite transformation with varying the prior austenite grain size in low carbon steel. *Metals* 8(12): 988. DOI: 10.3390/met8120988

23. Toloui, M. 2015. *Microstructural evolution in the HAZ of X80 linepipe steel phase field modelling*. Ph.D. dissertation. Vancouver, The University of British Columbia.

24. Huda, N. *Effect of martensite-austenite (MA) on mechanical properties of X80 linepipe steel*. Ph.D. dissertation. Waterloo, University of Waterloo.

25. Huda, N., Midawi, A., Gianetto, J. A., and Gerlich, A. P. 2021. Continuous cooling transformation behaviour and toughness of heat-affected zones in an X80 line pipe steel. *Journal of Materials Research and Technology* 12: 613-628. DOI: 10.1016/j.jmrt.2020.11.011

HANWEN YANG (*h376yang@uwaterloo.ca*), **NAZMUL HUDA**, **XIAOYE ZHAO**, and **ADRIAN P. GERLICH** are with the Centre for Advanced Materials Joining (CAMJ), Department of Mechanical and Mechatronic Engineering, University of Waterloo, Waterloo, Ontario, Canada. **JAMES CHEN** is with CanmetMATERIALS, Natural Resources Canada, Hamilton, Ontario, Canada.